Scholarly Research Exchange

Volume 2009 • Article ID 309529 • doi:10.3814/2009/309529

Research Article

An Experimental Study of Thermal Fatigue on ASTM A 213 Grade T-23 Steel Tube

G. R. Jinu,[1] P. Sathiya,[1] G. Ravichandran,[2] and A. Rathinam[2]

[1] *Department of Production Engineering, National Institute of Technology, Tiruchirappalli-620 015, Tamil Nadu, India*
[2] *Welding Research Institute, Bharat Heavy Electricals Limited, Tiruchirappalli-620 014, Tamil Nadu, India*

Correspondence should be addressed to G. R. Jinu, gr_jinu2002@yahoo.co.in and P. Sathiya, psathiya@nitt.edu

Received 9 January 2009; Revised 12 May 2009; Accepted 20 July 2009

Super heater tubes are subjected to alternate heating and cooling in power plants causes crack and eventually fail. This phenomenon is termed as thermal fatigue. In this paper, a laboratory simulation for reproducing thermal fatigue phenomenon is developed to determine the number of cycles of failure occurs in super heater tubes. Thermal fatigue tests are conducted in Non-Destructive Tested T23 base and SMAW welded tubes separately. The tubes are subjected to thermal cycles from 800°C (accelerated temperature) to room temperature (28°C). In this work 800°C is selected in order to achieve the crack much earlier. The selected temperature is just below the Ac_1 temperature. The tubes are subjected to heat by Oxy-acetylene flame and subsequently quenched with water. The tests are carried out until open cracks are identified. Surface cracks are identified in the base and weld tubes after 120 and 80 cycles respectively. The tubes are then sectioned and subjected to optical microscopy. The causes of failures are thoroughly investigated using Scanning Electron Microscope (SEM). This study reveals that localised heating and cooling causes thermal fatigue which initiates cracks in the tubes.

1. Introduction

T23 tubes are widely used in pressure part applications in boiler fired by fossil fuels and also in heat recovery steam generators. The creep-rupture properties of grades T22 and T23 have been compared for the temperature range of 500–650°C and the results show that grade T23 has a temperature advantage of approximately 50°C over grade T22. Thermal fatigue is a form of failure that occurs in components subject to alternate heating and cooling. Under thermal fatigue, crack can initiate, propagate, and eventually failure occurs. The reason for cracking is due to the temperature change in the material that induces thermal expansion (or contraction). If surrounding material or external constraints hinder this expansion, thermal stresses arise. These cyclic thermal stresses cause fatigue similar to that of mechanical stresses. This type of failures usually occurs in power industries where turbulent mixing of fluids causes quick thermal transients in boiler heat exchanger tubes as shown in Figure 1 [1].

Headers are an integral part of boilers. High-temperature steam-carrying headers are of significant concern in boilers because they have a finite creep life. The high-temperature headers include the superheater and reheater outlets, which operate at temperatures in excess of 600°C. These headers experience the effects of creep under normal operating conditions. In addition to the material degradation resulting from creep, high-temperature headers can also experience thermal and mechanical fatigue. Creep stresses combined with thermal fatigue stresses can lead to a failure much earlier than creep acting alone [3]. In addition to the effects of temperature variations, the external stresses associated with header expansion and piping loads must be included. In a boiler unit, header expansion may result in fatigue cracks at support attachments, moment restraints, superheater and reheater tubes, and header tubes to stub welds [3]. Failures are reported in critical boiler header components subject to thermal fatigue load applied in pressure vessels [4, 5]. From the above literatures, it is clearly identified that failures may take place in superheater tubes due to thermal fatigue.

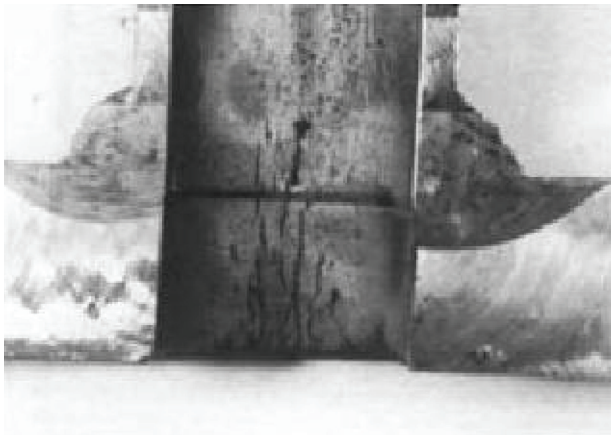

Figure 1: Sample piece of economizer inlet header showing crack in header hole and tube connector [1].

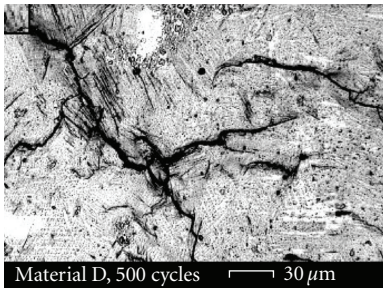

Figure 2: Microcracks [2].

Hence, it is important to study the effect of thermal fatigue on superheater tubes.

Virkkunen [2] conducted experiments on thermal fatigue of austenitic and duplex stainless steels subject to cyclic thermal transients in the temperature range 20°C to 600°C. They conducted experiments by heating the specimens rapidly using high-frequency induction coils and cooled by water spray. The specimens were rotated to achieve uniform heating and cooling. After 500 cycles, microcracks were formed in the sample and soon cracks formed a mosaic-like network which is typical for thermal fatigue as shown in Figures 2 and 3, respectively. The obtained thermal fatigue data was compared with the ASME pressure vessel code (1995) and design curve gives a safe design life for thermal fatigue loading. Similar type of mosaic-like network is obtained in this work also, which indicates the crack developed is due to the thermal fatigue process and not by any other means.

Kerezsi et al. [9] developed an experimental setup to conduct thermal fatigue using furnace and quenching rig on a plain carbon steel plate. They studied complex nonlinear stress distributions and environmental effects occurring during thermal shocks and they compared the results with ASME Boiler and pressure vessel code, Section VIII, Division 2 (1998), fatigue data curve as a guide line. The result shows good agreement with the design curve.

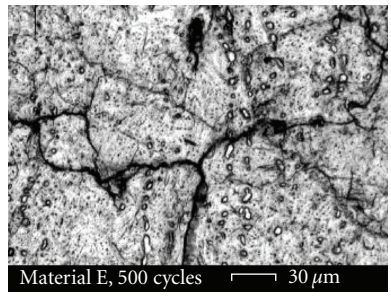

Figure 3: Mosaic-like network which is a typical thermal fatigue crack [2].

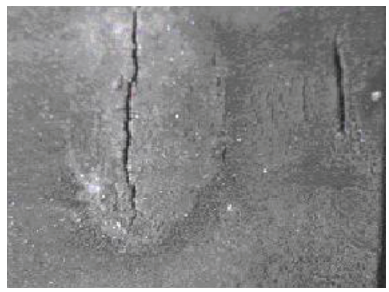

(a) Visual examination of microcracks [6]

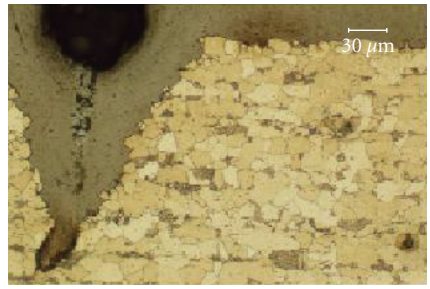

(b) Microcracks observed using optical microscopy [6]

Figure 4: Microcracks obtained in the failed sample.

Y. H. Choi and S. Y. Choi [10] have evaluated the integrity of socket weld in nuclear piping under the fatigue loading and deflection due to vibration on 304 SS and 316 SS material. The pressure transient ranging from P = 0 to 15.51 MPa and thermal transient ranging from T = 25°C to 288°C were applied. The stress distribution near a socket weld was studied using finite-element method and they compared the results with ASME code, Section III, (2001). Usman and Khan [6] analyzed the failure of T11 heat exchanger tubes used in ammonia plant that was subjected to thermal fatigue from 850°C to room temperature (25°C). They selected 850°C because these superheater tubes are exposed to the process gas temperature of 960°C. They conducted experiments to confirm the site failure results. After 100 thermal cycles, the cross-section of the tube was examined. The microfissures observed in the samples had a

close resemblance with cracks observed in the received failed tubes are shown in Figures 4(a) and 4(b).

Similar type of failure has occurred in this work, which indicates the crack developed is due to the thermal fatigue. Shiblia and Starr [11] discussed the new high-strength martensitic steel T91 issues and compared some of the perceived benefits with the actual plant experience under creep-thermal fatigue conditions. They suggested that for thin section components, the use of the T91 or other 9Cr martensitic steel tubing is not recommended due to their high level of steam side oxidation and other related oxide characteristics. Brown [12] developed a hybrid method using finite-element method to analyse the creep-fatigue life of boiler components. The developed method provides sufficient conservatism while still maintaining economically designed components for combined cycle gas-fired stations subject to rapid start up and cooling transients. The work also suggests the use of the finite-element method for thermal, stress-analysis aids in the correlation between operational events, and damage mechanisms. King and Riley [7] discussed about their recent experience in the condition assessment of boiler header components used in fossil-fired power plants. The work mentions many hurdles that may happen in boilers including internal borehole and ligament cracking and external tube connector weld cracking during operation as shown in Figures 5 and 6.

They concluded that the failure of headers are due to the material degradation resulting from creep, high-temperature headers which also experiences thermal and mechanical fatigue. This literature shows that thermal fatigue is one of the causes for the failure of headers and superheater tubes.

Paterson and Wilson [13] presented a number of practical examples where component life monitoring has been implemented on power plants particularly in high-temperature boiler headers and turbines. Headers are subject to the damage mechanisms of creep due to onload temperature and pressure. Fatigue failures are due to start up and shutdown where thermal transient occurs which is similar to this present work. They developed a damage-monitoring system to give substantial benefits to operators in terms of damage reduction and quantitative life assessment. Tokiyoshi et al. [14] has carried out thermal fatigue test on perforated plate. The plate was examined under the high pressure and high thermal stresses during plant operations for prediction of creep fatigue life, finite-element method (FEM) was carried out and compared with experimental results.

Kerezsi et al. [15] developed a test method for analyzing the initiation and growth of cracks in pressure vessels and piping equipment. This method simulates the repeated thermal shock conditions produced in operating thermal power station equipment. The work suggests that the primary stress has little or no effect on crack initiation lifetime during repeated thermal shock below the creep range and the environmental interaction is highly influential in the growth of thermal shock cracks. The work also compares the experimental results with prediction methods from the ASME Bolier and pressure vessel code, Section VIII, Division 2 (1998). Smith et al. [8] had simulated a laboratory procedure

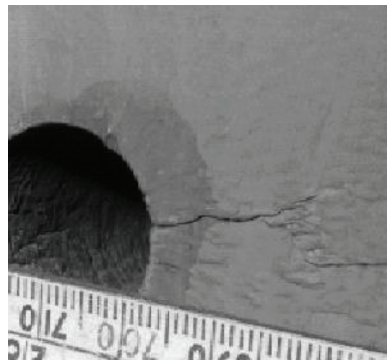

Figure 5: Closeup view of inside surface header sample piece showing cracking [7].

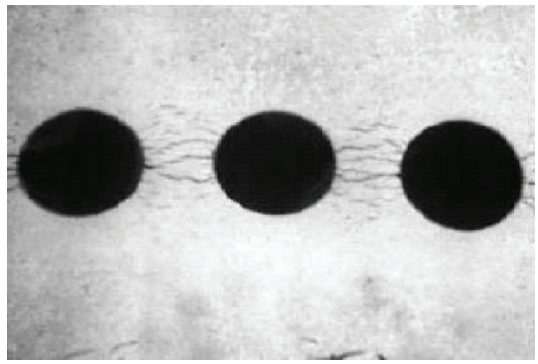

Figure 6: Inside surface of economizer inlet of header showing circumferential ligament field and borehole cracking [7].

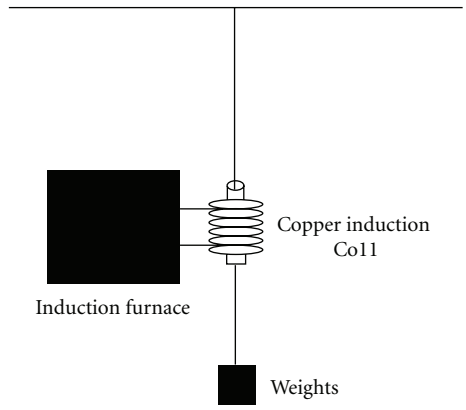

Figure 7: Experimental set up employed by Smith et al. [8].

using induction coil and quenching rig for reproducing high-temperature cracks found in coal-fired boiler tubes as shown in Figure 7. They proposed that the crack initiation is by an intergranular surface corrosion/thermal stress interaction mechanism and environmentally assisted thermal fatigue crack propagation as shown in Figure 8.

Underwood and Banerji [16] have analyzed the failure caused in a 101-C ammonia plant heat exchanger tubes. They suggested that the failures are due to the formation and

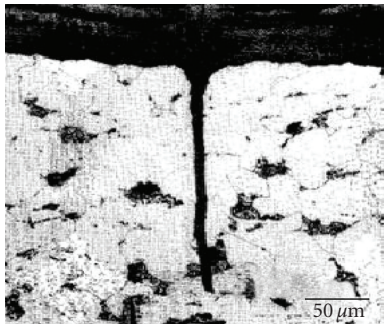

Figure 8: Microcracks obtained by Smith et al. [8].

growth of internal oxide scales or deposits at areas of high heat flux. They presented a case history involving thermal fatigue type of failure. They analyzed the failures using finite-element modeling.

From the above literatures, it is clearly found that thermal fatigue is an important phenomenon for the development of cracks in pressure vessel components especially in super-heater tubes. Many works were already done in studying the influence of thermal fatigue on failure of boiler headers using FEM. However, simulating the thermal fatigue behaviour using laboratory setup is available with some constraints (dimensions and other conditions).

The objective of this paper is to study the effect of thermal fatigue on base, welded tubes and to determine the numbers of cycles of failure. In this work, a laboratory simulation reproducing thermal fatigue phenomenon is developed and thermal fatigue tests are conducted in both base and weld tubes separately. The tubes are subject to thermal cycles from 800°C to room temperature. The tests are carried out until open cracks are identified. The cause of the failure is thoroughly investigated in this paper.

2. Experimental Work

2.1. Specimen Preparation. Two attested ASTM A 213 grade T-23 tubes of 300 mm length, 45 mm outer diameter, and 10 mm thickness are taken for this experimental study. One of the tube is taken as base tube as shown in Figure 9.

Another tube is sectioned into two equal halves of 150 mm length and then edges are prepared for butt-welding. The joint designs are selected as a single "V" joint. The edge preparation angle is 30° and the root face is 1 mm as shown in Figure 10. The joint fit up is tacked with MMAW as shown in Figure 11.

The tack-welded tube is preheated to 220°C by GTAW preheating method. The root is GTA welded with TGS 2 CW filler wire with 85-ampere current and voltage of 17 V is used in this study. The first and the second fill passes are welded with stick electrodes of 2.5 mm and 3.2 mm in diameter with 90–115 amperes, while the remaining three passes are welded by SMAW process with thermanit 23 electrodes of 125–135 amperes current. The necessary preheating is done at 220°C for 57 seconds. After the completion of the welding, radiographic examination is done to ensure the quality of welds and the results are found to be acceptable range as per the ASME pressure vessel code requirements. The welded tube is shown in Figure 12.

The chemical composition and mechanical properties of the T23 tube, T23 filler wire and electrode are given in Tables 1 and 2, respectively.

The microstructures of the base tube before subject to thermal fatigue is shown in Figure 13. The microstructures of the welded tube before subject to thermal fatigue is shown in Figures 14(a) and 14(b).

From Figure 13, T23 base tube has a bainitic-martensitic structure. It is a result of precise heat treatment operation after heating the metal to above Ac_3 temperature. Ac_1 is located between 800°C and 820°C, and Ac_3 temperature is between 960°C and 980°C. The cooling rate for T23 is 200 K/s. After the bainitic-martensite structure is formed it is normalized at 1060°C for the dissociation of most of the precipitates. Tempering at 760°C allows the growth of precipitates like chromium carbide, vanadium and niobium carbonitrides, and so forth. This process helps to improve creep resistance at high-temperatures. The grains are little coarse and irregular in shape. The high strength of this alloy comes from the bainitic structure. It is a mixture of bainite and martensite with little delta ferrite to give the required ductility. The carbides that are formed in the grain boundaries that will give the necessary strength and the bainite give the hardness. The grain boundaries are clearly visible but the grain growth is irregular producing an irregular structure.

The microstructures of weld tube before subject to thermal fatigue are shown in Figures 14(a) and 14(b).

The difference in the grain size can be seen in the above microstructure. The dark-colored patch indicates the bainite-martensite structure. The white areas indicate the delta ferrite. When compared to the base the weld contains more delta ferrite structure. From Figures 14(a) and 14(b) it is observed the grains are very fine in the base material Figure 14(a) and the weld Figure 14(b) shows coarse grains.

2.2. Experimental Setup. An apparatus has been purposed by built to conduct thermal fatigue tests. The test set-up employed in this study consists of the following main physical components:

(1) the oxy-acetylene heating set up,

(2) the specimen mounting frame,

(3) the specimen holding system,

(4) quenching rig,

(5) laser sensor temperature measuring system.

The specimen is locally heated up by Oxy-acetylene flame from the outer surface of the tube. The peak temperature can be suddenly attained by this process. The experimental setup is shown in Figure 15.

2.2.1. Oxy-acetylene Heating Setup. The Oxy-acetylene heating set up is used as a heating source. The oxygen and acetylene pressure is regulated to 0.5 and 1 bar, respectively.

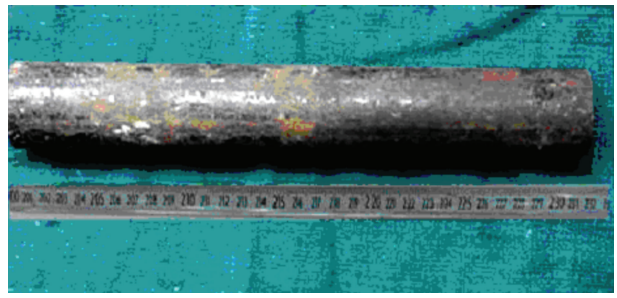

Figure 9: T-23 base tube before subject to thermal fatigue.

Table 1: Chemical composition of ASTM A 213 GRADE T-23 material and T23 filler wire and electrode.

Materials	Elements (wt%)													
	C	Mn	P	S	Si	Cr	Mo	V	W	Nb	B	N	Al	Ni
ASTM A 213 GRADE T-23	0.04–0.10	0.10–0.60	0.03	0.01	0.50	1.92–2.60	0.05–0.30	0.20–0.30	1.45–1.75	0.02–0.08	.0005–.0060	0.03	0.03	—
GTAW filler wire	0.08	0.54	—	—	0.27	2.14	0.08	0.21	1.58	0.031	.002	.011	—	0.04

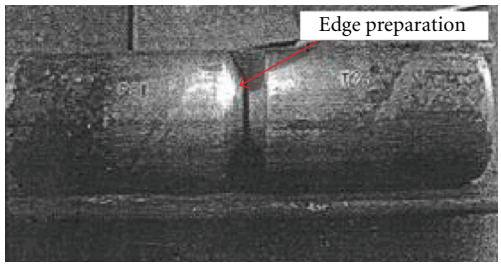

Figure 10: Specimen after edge preparation.

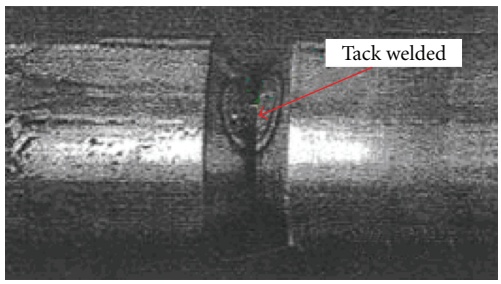

Figure 11: Specimen after tack welding.

Figure 12: Weld specimen before subjected to thermal fatigue.

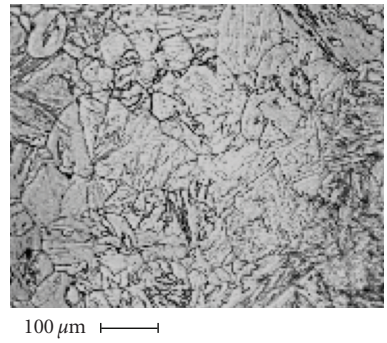

Figure 13: Microstructure of base before subject to thermal fatigue.

As shown in Figure 16, the oxy-acetylene flame is moved in clockwise direction from point "A" and ends at the same point. The torch is continuously shown in the heating surface until 800°C is attained. Time taken to attain 800°C is 5 minutes.

2.2.2. Specimen Mounting Frame. As shown in Figure 16, two ends of the tube are welded with a thick ridge plate and then the two plates are welded with a bottom plate so that the linear expansion of the tube during heating is arrested. A steel rod is welded on the top surface of the plate for holding the specimen mounting frame to immerse it in the quenching rig.

2.2.3. Specimen Holding System. The specimen holding system consists of leverage to handle the hot specimen for immersing it in the quenching rig as shown in Figure 17.

2.2.4. Quenching Rig. The quenching rig consists of a tank filled with water. After the completion of the heating cycle,

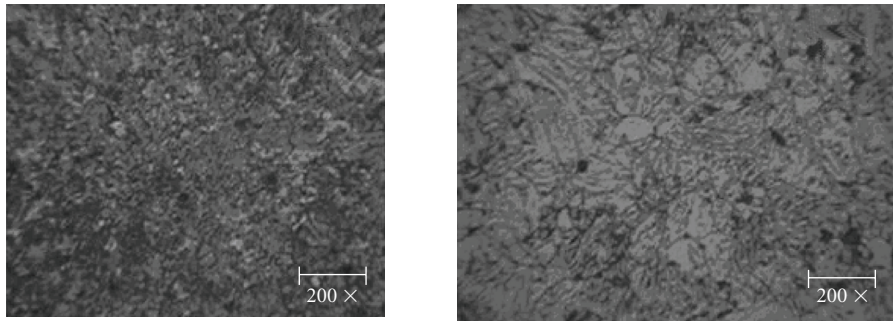

(a) (b)

Figure 14: Microstructure of base (a) and weld (b) regions in the weld tube before subject to thermal fatigue.

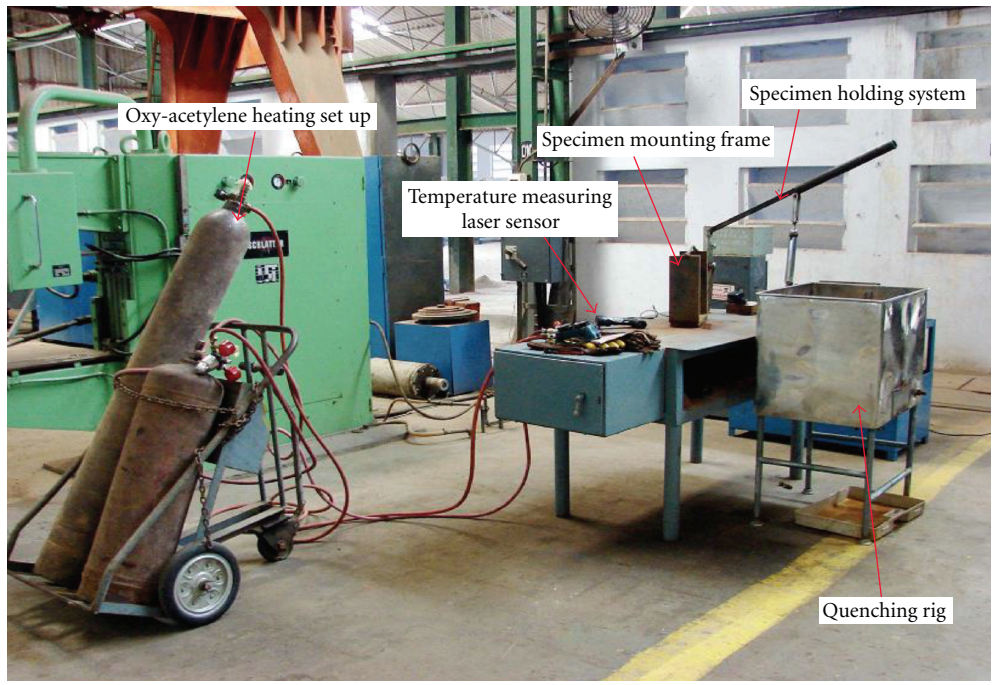

Figure 15: Experimental setup.

the specimen is immersed in the quenching rig with the help of holding system as shown in Figure 17. The temperature of the specimen is suddenly decreased to room temperature after 5 minutes.

2.2.5. Temperature Measuring Laser Sensor. The temperature is measured using laser sensor at the end of every cycle to check whether 800°C is attained or not.

2.3. Experimental Procedure. The specimen is prepared as discussed above and heat is applied from the outer surface of tube, which are the actual conditions of a heat exchanger tube exposed to the thermal fatigue on pressure vessels. The flame is shown in the heating zone manually, starting from one point of the heating zone and ends in the same point so that heat will be locally distributed from the outer surface tube to the inner surface as shown in Figure 16. After heating, the temperature of the specimen is measured using laser thermometer to check whether the attained temperature reaches 800°C. The time taken to attain 800°C is 5 minutes. The flame is then turned off. Then the hot specimen is lifted with the help of the specimen-holding system and immersed into the quenching rig. The specimen is taken out from the quenching rig when the temperature of the specimen reaches the room temperature. All of the above processes constitute one thermal fatigue cycle. For one thermal cycle, 10 (5 + 5) minutes are taken which include both the heating and the cooling cycle. The experiments are conducted until open cracks are identified. The specimen is then removed from the specimen-mounting frame, NDT test is carried out, and the specimen is then sectioned for metallographic study.

Table 2: Mechanical properties of ASTM A 213 GRADE T-23 material and T23 filler wire and electrode.

Materials	Ultimate tensilestrength, UTS MPa	0.2%Yield strength, YS MPa	% of Elongation
ASTM A 213 GRADE T-23	510	400	20
GTAW filler wire	620	520	20.2
SMAW Electrode	553	421	25

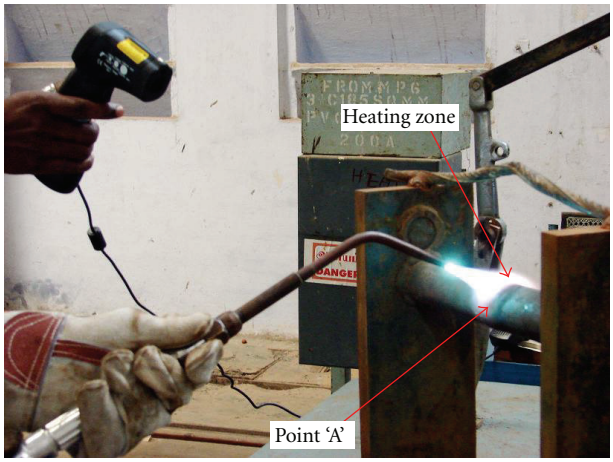

Figure 16: Specimen mounting frame with heating.

3. Results and Discussion

The experiments are carried out until open cracks were identified. Surface cracks are identified in the base and weld tubes after 120 and 80 cycles, respectively.

3.1. Visual Inspection in Failed Tubes. The failed base and weld tubes are visually inspected. The developed crack in the tubes are measured and presented in what follows.

3.1.1. Visual Inspection in Failed Base Tube. The macrograph of the failed base tube is shown in Figure 18. From Figure 18, it is observed that many surface cracks are obtained in the base tube subjected to thermal fatigue after 120 cycles. A 20 mm long longitudinal crack is visually identified in the failed base tube at the heated zone. The tube is bulged in the heating zone due to localised heating. The failed tube is then subjected to liquid penetrant test to identify the small surface cracks.

3.1.2. Visual Inspection in Failed Weld Tube. The macrograph of the failed weld tube is shown in Figures 19(a) and 19(b). From Figures 19(a) and 19(b), it is observed that many surface cracks are present in the base tube subjected to thermal fatigue after 80 cycles.

Transverse cracks of 80 mm long are visually identified in the failed weld tube at the heated zone.

3.2. Liquid Penetrant Test. To identify the small surface cracks on the failed tubes, the base and weld tubes are subjected to liquid penetrant test.

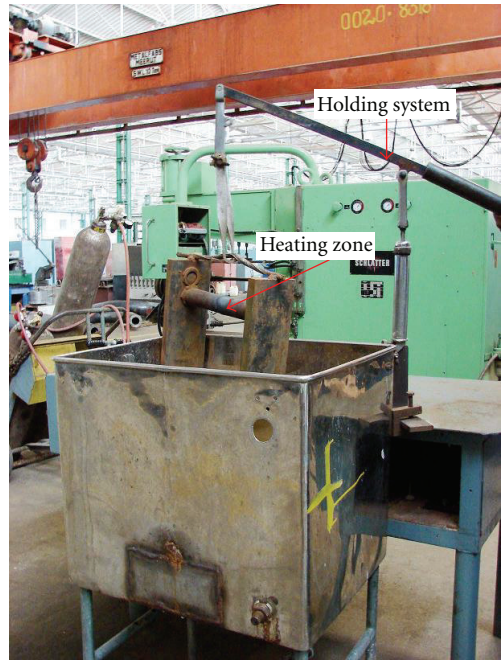

Figure 17: Specimen holding system and quenching rig.

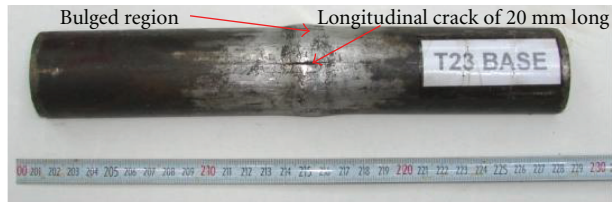

Figure 18: Visual inspection of failed base specimen after subjected to thermal fatigue.

3.2.1. Liquid Penetrant Test on Failed Base Tube. The macrograph of the failed base specimen subjected to liquid penetrant test is shown in Figure 20 and it clearly shows that many longitudinal cracks are found in the heated zone and from the longitudinal crack, small transverse cracks are also identified, which were not seen in the visual examination.

3.2.2. Liquid Penetrant Test on Failed Weld Tube. Figure 21 shows the macrograph of the failed weld specimen subjected to liquid penetrant test and it clearly shows that many transverse cracks are developed in the heated zone which propagates through out the circumference of the weld and from the transverse crack small longitudinal cracks are also seen which were not seen in the visual examination.

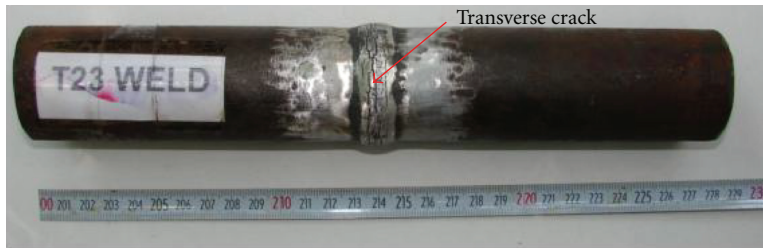

(a)

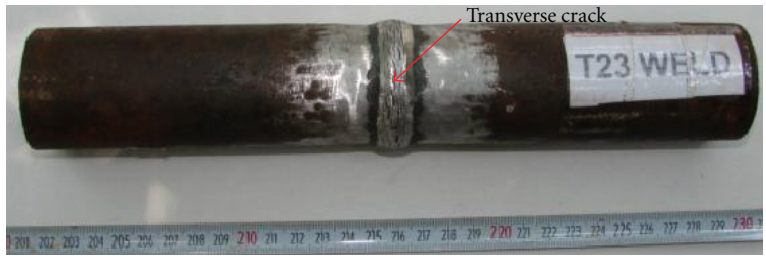

(b)

Figure 19: Visual inspection of failed weld specimen after subjected to thermal fatigue.

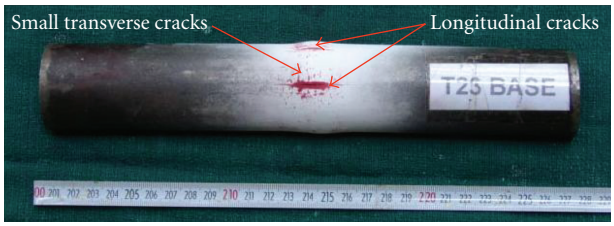

Figure 20: Liquid penetrant examination of failed base specimen.

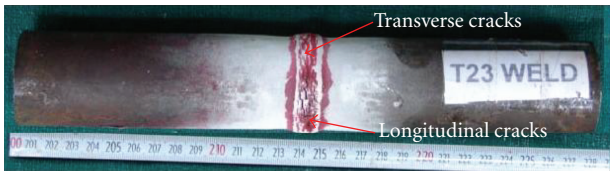

Figure 21: Liquid penetrant examination of failed weld specimen.

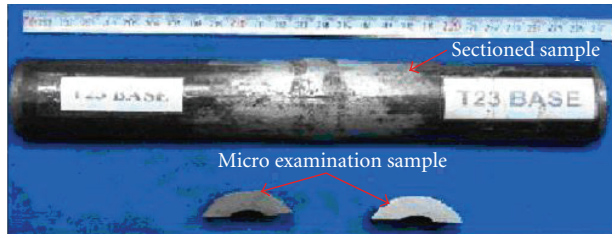

(a)

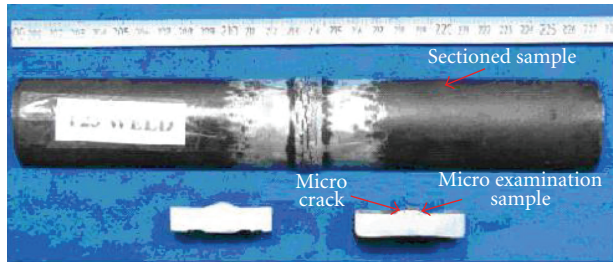

(b)

Figure 22: Sectioned view of the failed base and weld tubes.

The failed tubes are then sectioned and subjected to metallographic study.

3.3. Specimen Preparation for Metallographic Study. The sectioned view of the failed base and weld tube is shown in Figures 22(a) and 22(b). The failed tubes are sectioned in two halves in longitudinal direction and again one half of the tube is divided into two sections. The projected portion from the two sides of the heating zone in the tube is removed further so that only the heat-affected zone is taken for metallographic study. Specimens for metallographic examinations are prepared by polishing successively in 220, 320, 400, 600, 800 emery grits, followed by a cloth disc polishing. The specimens are etched with 2% Nital solution.

The specimens are then subjected to microscopic and SEM study and the results are discussed.

3.4. MacroStudy. Before examining in the microanalysis the polished samples are examined to macroscopically study. The macrophotographs are taken in the outer surface of the failed tubes to get the closer view possible of the cracks obtained in the surface while the microstructure are taken in the cross-section of the failed tube to study the depth of penetration of the crack.

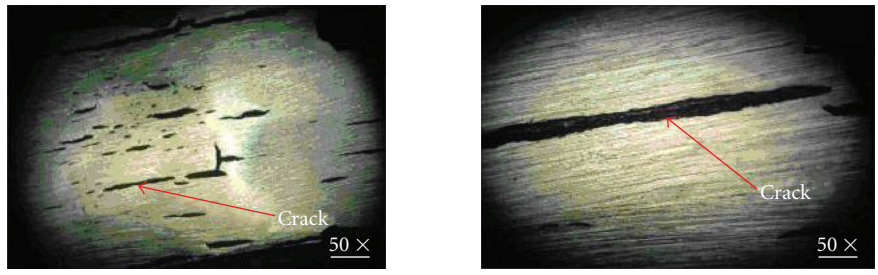

(a) (b)

Figure 23: Surface crack obtained in the failed base tube.

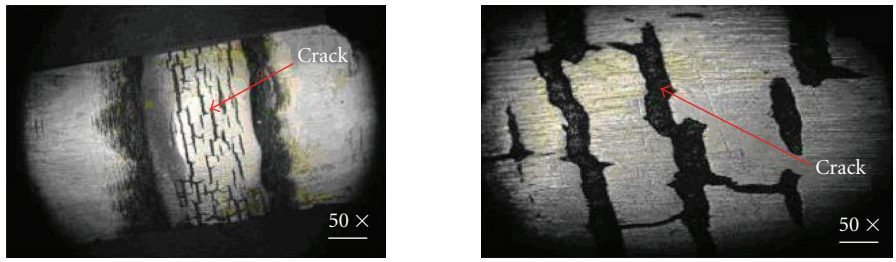

(a) (b)

Figure 24: Surface crack obtained in the failed weld tube.

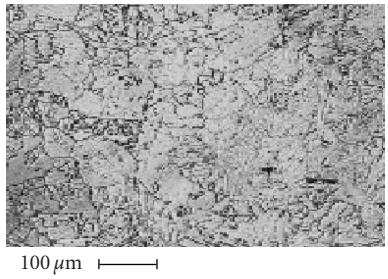

Figure 25: Microstructure of the failed base in defect free region.

Table 3: Hardness taken in the base tube (HV, 10 kg).

Position	Base	Heating Zone	Near the Crack
Before subjected thermal fatigue	258,260	—	—
After failure occurs	252,254	327,327	339,334

3.4.1. Macrostudy on the Failed Base Tube. Figure 23(a) shows the magnified view of the surface crack obtained in the failed base tube subjected to thermal fatigue and it is clearly identified that many longitudinal cracks are found in the heated zone, and from the longitudinal crack small transverse cracks are also developed. Figure 23(b) shows the magnified view of the single longitudinal crack obtained in the failed base tube.

3.4.2. Macrostudy on the Failed Weld Tube. Figure 24(a) shows the magnified view of the surface crack obtained in the failed weld tube subjected to thermal fatigue and it is clearly identified that many transverse cracks are found in the weld joint, and from the transverse crack small longitudinal cracks are also developed. Figure 24(b) shows the magnified view of the surface crack obtained in the failed weld tube.

3.5. Optical Microscopy. The samples are prepared according to the ASME standards. The polished and etched samples are examined under optical microscopy and SEM. The microstructures are taken on different locations of the tubes in the defect and defect-free surfaces.

3.5.1. Study on the Failed Base Tube. The metallographic samples prepared from the failed base tube are studied thoroughly by optical microscope in both the defect and defect-free regions.

(1) *Study on the Defect Free Surfaces on the Failed Base Tube.* The microstructures of defect-free surfaces of the failed base tube are shown in Figure 25.

Figure 25 shows the optical microstructure of failed base tube taken in the defect free surface. The microstructure of T23 failed base tube shows that the grains are little coarse and irregular in shape. The failed thermal fatigued base tube shows similar microstructure as observed in the base tube before being subjected to thermal fatigue. This reveals that during thermal fatigue there is no phase transformation taking place in the base tube subjected to thermal fatigue.

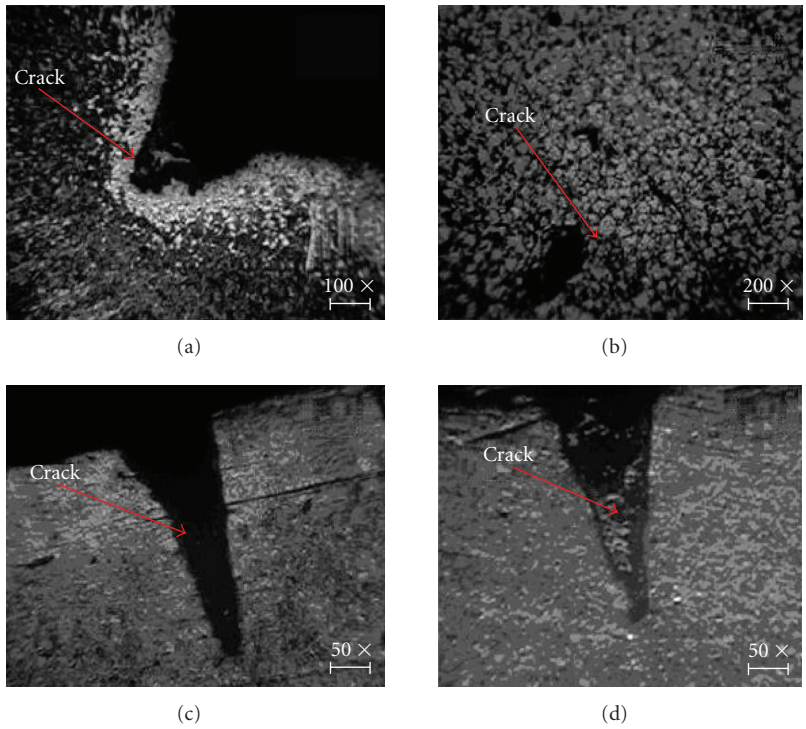

Figure 26: Cracks identified in the failed base tube.

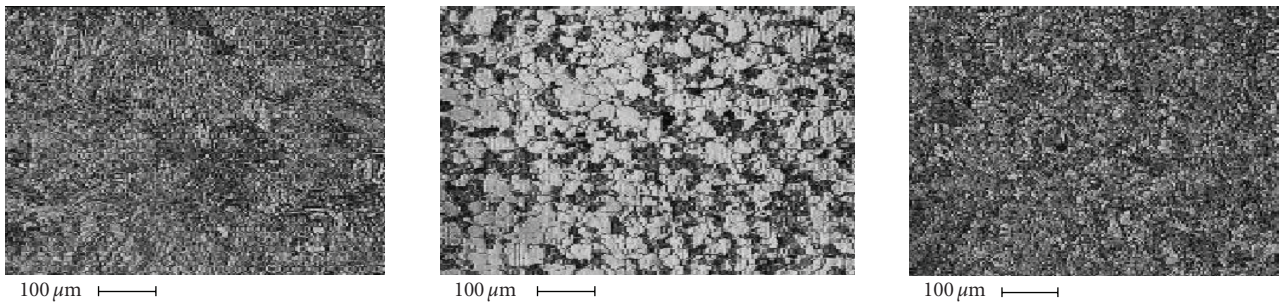

(a) Weld metal after thermal fatigue in outer surface.

(b) Weld metal after thermal fatigue in inner surface.

(c) Weld metal after thermal fatigue in HAZ.

Figure 27: Microstructure of weld region in defect free areas of the failed weld tube.

(2) *Study on the Defect Surfaces on the Failed Base Tube.* Through the optical microscope, the defect surfaces in the T23 base tube are identified and presented in Figures 26(a)–26(d). From the Figures 26(a)–26(d) it is clearly identified that large number of cracks are present in the failed base tube. The cracks have developed from the heating surface (outer surface) of the tube and propagate towards the inner surface. Cracks are observed in the failed base tube have a close resemblance with cracks observed in the failed tubes [6]. In Figure 26(a), mild decarburization to the depth of one grains is observed. The obtained cracks in the failed base tubes show blunt tip cracks as shown in Figure 26. This crack shows typical characteristics of thermal fatigue failure.

3.5.2. Study on the Failed Weld Tube. The metallographic samples prepared from the failed weld tube are studied thoroughly by optical microscope in both the defect and defect-free regions.

(1) *Study on the Defect Free Surfaces on the Weld Tube.* The microstructures of defect-free surfaces of the failed weld tube are shown in Figures 27(a) and 27(c). The microstructures of the weld are taken on the outer surface, HAZ, and inner surface of the tube as shown in Figures 27(a) and 27(b). When compared to the grains observed in inner surface of the tube, the outer surface and HAZ shows very finer grains. This difference is due to the application of the heat from the outer surface of the tube to the inner surface. Formation of martensite is more as observed in the failedwelded tubes when compared to the base tubes.

(2) *Study on the Defect Surfaces on the Weld Tube.* Through the microstructures, the defect surfaces in the weld tube is identified and presented in Figures 28(a)–28(e). From Figures 28(a)–28(e), it is clearly identified that large number of cracks are present in the failed weld tube. The cracks are developed from the heating surface (outer surface) of

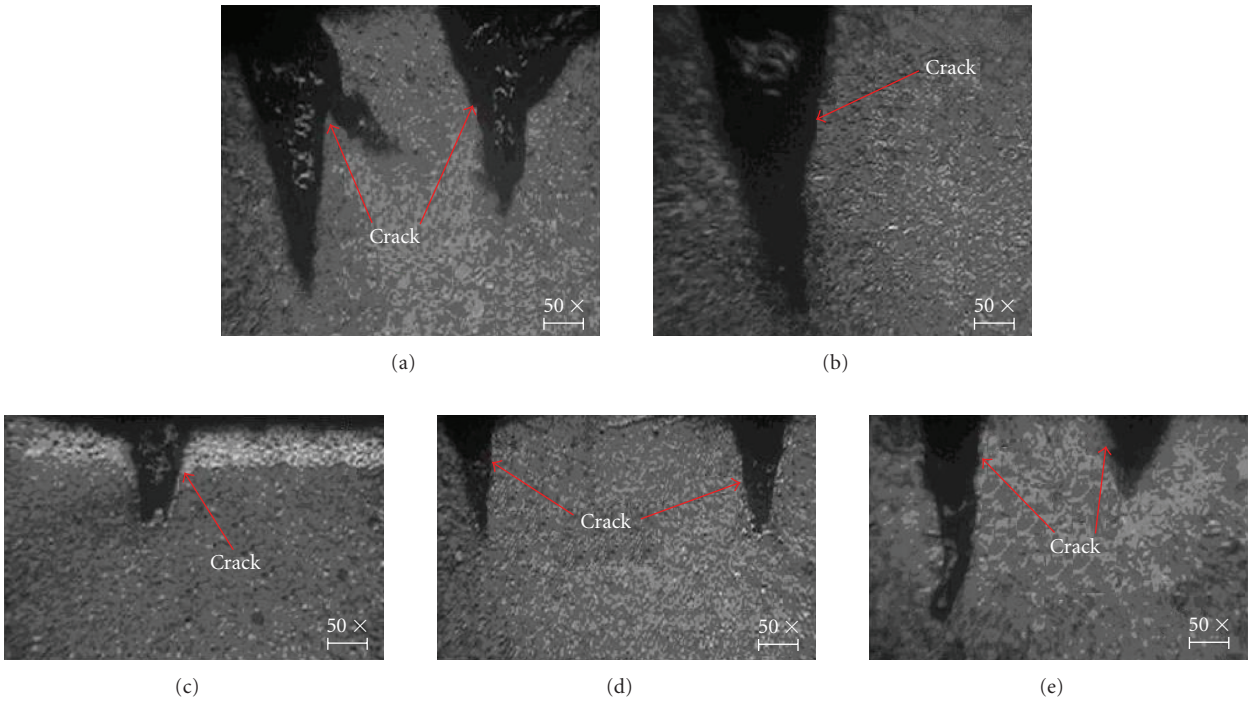

Figure 28: Cracks identified in the failed weld tube.

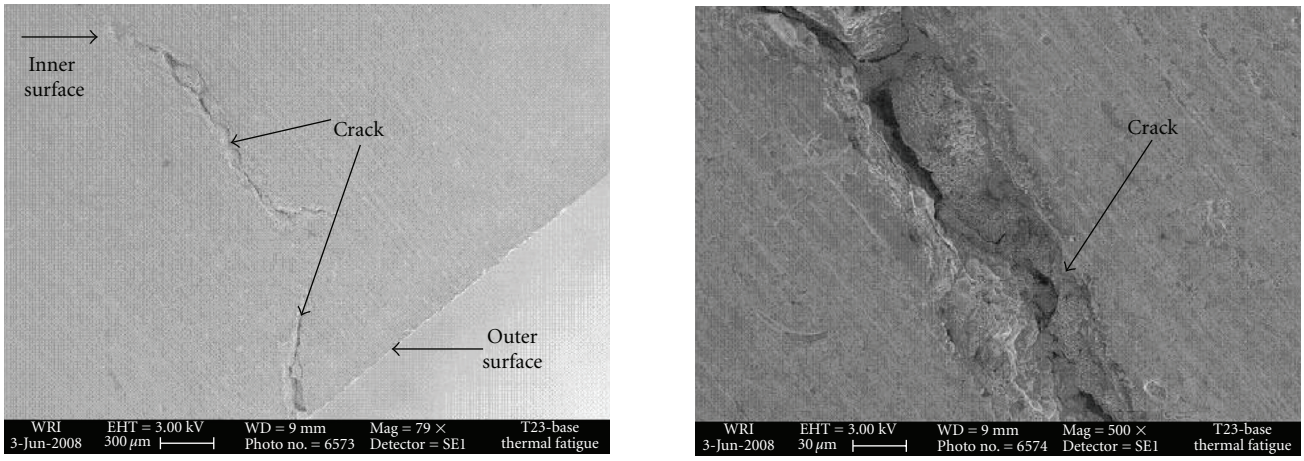

Figure 29: Crack propagation in the failed base tube.

the tube and propagate towards the inner surface. Cracks observed in the weld tube which had a close resemblance with cracks observed in the failed tubes as reported in [6]. The obtained cracks in the failed base tubes show that blend tip cracks and parallel cracks are also observed as shown in Figure 28. This crack shows typical characteristics of thermal fatigue failure.

3.6. SEM Study. The cracks observed with the optical microscope have been observed with an SEM study to analyse the failures in detail. SEM analyses are carried out in defect surfaces of the base and weld tube.

3.6.1. Defect Surface on Failed Base Tube. The cracks observed in the SEM photography of the failed base tube are shown in Figures 29(a) and 29(b). From Figures 29(a) and 29(b), the cracks are developed from the outer surface of the tube and propagate towards the inner surface. Similarly it travels through or across the circumference of tube heated region. When it is compared to the cracks obtained in the failed weld tube, the width and depth of the cracks are less as shown in Figures 29(a) and 29(b). The cracks have been opened and examined as shown in Figures 30(a) and 30(b). They revealed smooth-oxidized crack surfaces. From Figure 31, Mosaic-like crack formation is observed when it is magnified. From Figures 29(a) and 29(b) it is clearly

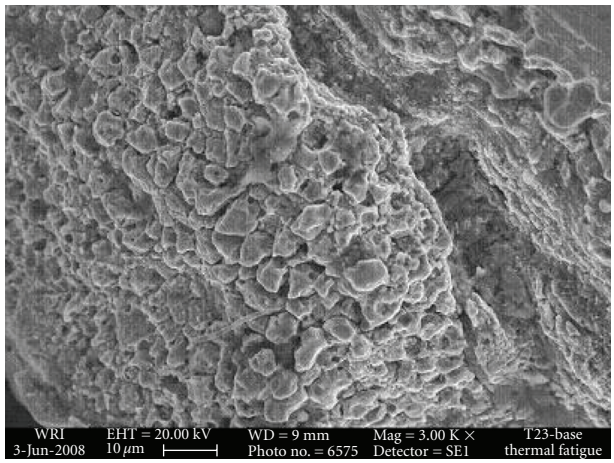

(a)

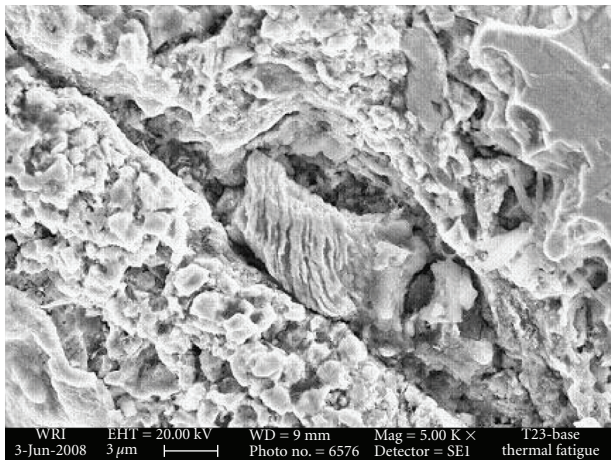

(b)

Figure 30: Smooth-oxidized crack surfaces.

identified that the initial position of the crack width is high, when it propagates towards the inner surface, the crack growth rate increases due to the temperature difference and rate of cooling. Due to these reasons, cracks are developed.

3.6.2. Defect Surface on Failed Weld Tube. Figure 32 shows the microstructure taken in an unaffected region of the failed weld tube. The defects present in the failed weld tube are shown in Figures 33(a) and 33(b). From Figure 33, the cracks are developed from the outer surface of the tube and propagate towards the inner surface. Similarly, it travels in the circumference of the tube-heated region. When compared to the base crack, the size of the crack obtained in the weld is large. Mosaic-like crack formation is observed when it is magnified as shown in Figures 34(a) and 34(b) which is a typical thermal fatigue crack. From Figures 33(a) and 33(b), the initial crack width is large, when it moves towards the inner surface, the crack growth rate increases due to the temperature difference and rate of cooling. Due to these reasons, cracks are developed.

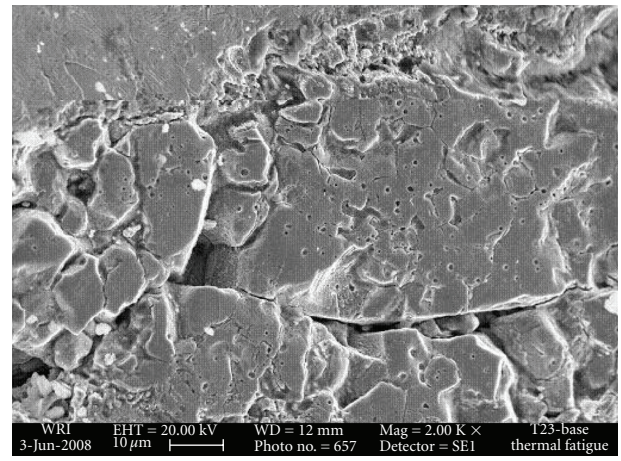

Figure 31: Mosaic-like crack formation.

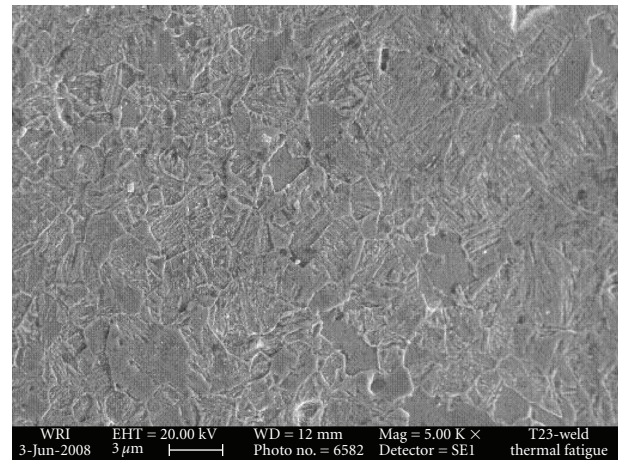

Figure 32: Unaffected weld tube structure.

On evaluating the microstudy and SEM results, it is clearly identified that the cracks are developed from the heating surface (outer surface) of the tube and propagate towards the inner surface, which eventually cause failure of the tube. The cracks occurring in the tube is due to long-time exposure in high service temperature. Mosaic-like crack formation is observed inside the crack at higher magnification. The cracks obtained in the tube specimen is the typical thermal fatigue crack which resembles the failures reported in tubes subjected to thermal fatigue [6].

3.7. Hardness. Vickers's hardness measurements are taken on the base and welded tube, before subjected to thermal fatigue and after failure occurs. The hardness location taken in the base and welded specimen is shown in Figures 35 and 36. The load applied is 10 kg and the hardness values taken in the base and welded specimen are tabulated in Tables 3 and 4.

From Tables 3 and 4, the hardness value is much higher nearer in the cracked zone. Due to the higher hardness, the initiated cracks due to the thermal fatigue can propagate towards the circumferential areas and through the thickness of the tube. The hardness value of the weld near the crack zone is nearly closer, due to repeated heating and cooling.

Table 4: Hardness taken in the weld tube.

Position	Base	Weld	HAZ	Heating Zone	Near the Crack
Before subjected thermal fatigue	264, 268	274, 282	296, 284	—	—
After failure occurs	333,333	360,348	339,351	360,348	370,360

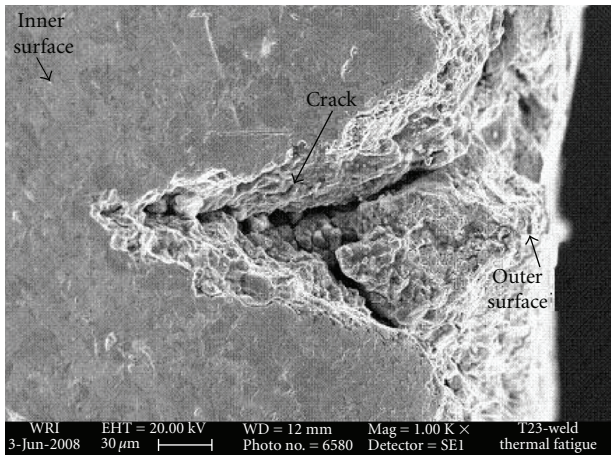

Figure 33: Crack propagation in the failed-welded tube.

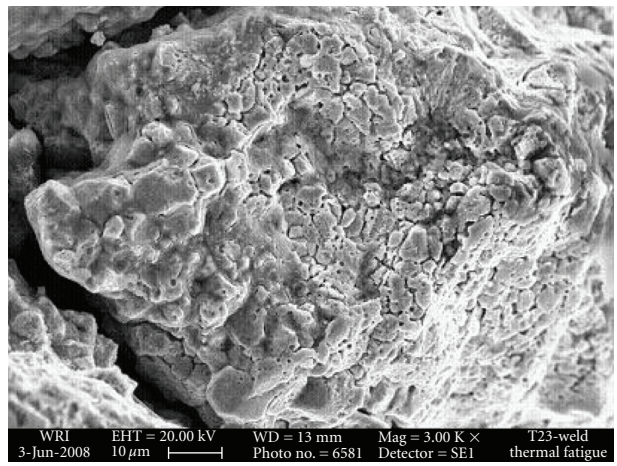

(a) Smooth-oxidized crack surfaces

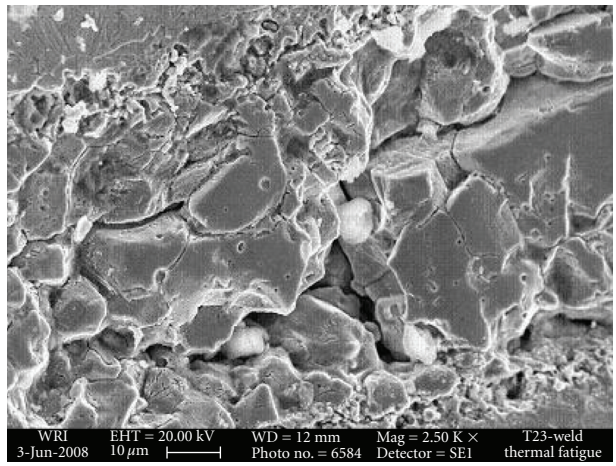

(b) Mosaic-like crack formation

Figure 34: Smooth oxidized crack surfaces and Mosaic-like crack formation.

The grains get finer near the outer surface of the tube where heat is applied which are discussed in micro structural study, hence hardness value increases when compared to the base material.

4. Conclusion

From this research work, the following conclusions are drawn

The effects of thermal fatigue on ASTM A 213 GRADE T-23 base, weld tubes are studied effectively and the number of cycles to failure occurs are obtained experimentally.

(1) While thermal cycling surface cracks are identified in the base and weld tubes after 120 and 80 cycles, respectively. This shows that the base tube will withstand 40 more cycles than the welded tubes subjected to thermal fatigue.

(2) From the visual examination a 20 mm long longitudinal crack are visually identified in the failed base tube in the heated zone. The tube is bulged in the heating zone which is clearly seen. A transverse crack of 80 mm long is visually identified in the failed weld tube at the heated zone. This shows that during thermal fatigue in the base tube, longitudinal crack is developed and in the welded tube transverse crack is obtained.

(3) Liquid penetrant test shows that apart from the longitudinal crack small transverse crack is also observed in the failed base tube. Similarly, in the welded tube apart from the transverse crack, small longitudinal crack is also observed in the failed-welded tube.

(4) From the macro- and the microexaminations, cracks are observed in the failed base and the welded specimens. The cracks have developed from the outer surface of the tube and propagate towards the inner surface of the tube.

(5) The SEM examination revealed smooth oxidized crack surfaces and Mosaic-like crack formation is observed inside the crack at higher magnification.

(6) The hardness test shows that at the point nearer to the crack, the hardness value is much higher. Due to the higher hardness cracks developed by the thermal fatigue process propagate toward the circumferential areas and through the thickness of the tube. The

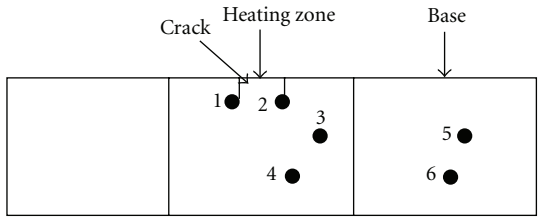

Figure 35: Hardness locations taken in the failed base tube.

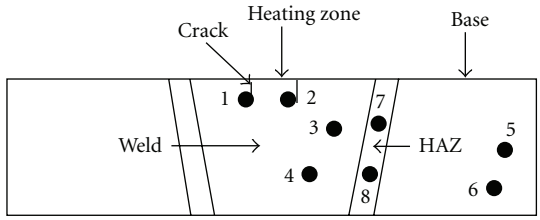

Figure 36: Hardness locations taken in the failed weld tube.

hardness values of the weld near the crack zone is nearly closer, because due to repeated heating and cooling, the grains get finer and the hardness values have increased when compared to the base material.

(7) The development of these cracks is due to the temperature variation from high-temperature to room temperature, which is similar in the power plant during the start-up and shut-down operations.

References

[1] M. Hayashi, "Thermal fatigue behavior of thin-walled cylindrical carbon steel specimens in simulated BWR environment," *International Journal of Nuclear Engineering and Design*, vol. 184, no. 1, pp. 123–133, 1998.

[2] I. Virkkunen, *Thermal Fatigue of Austenitic and Duplex Stainless Steels. Acta Polytechnica Scandinavica*, Mechanical Engineering Series no. 154, Finnish Academies of Technology, Espoo, Finland, 2001.

[3] T. Yoshimoto, S. Ishihara, T. Goshima, A. J. McEvily, and T. Ishizaki, "Improved method for the determination of the maximum thermal stress induced during a quench test," *Scripta Materialia*, vol. 41, no. 5, pp. 553–559, 1999.

[4] A. Tulyakov, "Thermal fatigue in heat power engineering," *Mashinostroyeniye*, vol. 197, 1978.

[5] A. B. Vainman, R. K. Melekhov, and O. D. Smiyan, *Hydrogen Induced Embitterment of High-Pressure Boiler Elements*, vol. 272, Naukova Dumka, Kyiv, Russia, 1990.

[6] A. Usman and A. N. Khan, "Failure analysis of heat exchanger tubes," *Engineering Failure Analysis*, vol. 15, no. 1-2, pp. 118–128, 2008.

[7] J. P. King and D. B. Riley, "Recent experience in condition assessment of boiler header components and supports," in *Proceedings of the ASME Pressure Vessels and Piping Conference*, vol. 333, pp. 135–140, July 1996.

[8] B. J. Smith, C. I. Erskine, R. J. Hartranft, and A. R. Marder, *High-Temperature Corrosion-Fatigue (Circumferential) Cracking Life Evaluation Procedure for Low Alloy Cr-Mo) Boiler Tube Steels*, Lehigh University, Bethlehem, Pa, USA, 1999.

[9] B. B. Kerezsi, J. W. H. Price, and R. N. Ibrahim, "Using S-N curves to analyse cracking due to repeated thermal shock," *Journal of Materials Processing Technology*, vol. 145, no. 1, pp. 118–125, 2004.

[10] Y. H. Choi and S. Y. Choi, "Socket weld integrity in nuclear piping under fatigue loading condition," *Nuclear Engineering and Design*, vol. 237, no. 2, pp. 213–218, 2007.

[11] A. Shiblia and F. Starr, "Some aspects of plant and research experience in the use of new high strength martensitic steel T91," *International Journal of Pressure Vessels and Piping*, vol. 84, pp. 114–122, 2007.

[12] T. B. Brown, "Assessing the effect of thermal transients on the life of boiler plant, Babcock energy limited," Scotland, 1998.

[13] I. R. Paterson and J. D. Wilson, "Use of damage monitoring systems for component life optimisation in power plant," *International Journal of Pressure Vessels and Piping*, vol. 79, no. 8–10, pp. 541–547, 2002.

[14] T. Tokiyoshi, F. Kawashima, T. Igari, and H. Kino, "Crack propagation life prediction of a perforated plate under thermal fatigue," *International Journal of Pressure Vessels and Piping*, vol. 78, no. 11-12, pp. 837–845, 2001.

[15] B. B. Kerezsi, A. G. Kotousov, and J. W. H. Price, "Experimental apparatus for thermal shock fatigue investigations," *International Journal of Pressure Vessels and Piping*, vol. 77, no. 7, pp. 425–434, 2000.

[16] E. E. Underwood and K. Banerji, "Fractal analysis of fracture surfaces," in *ASM Hand Book*, vol. 12, Metals Hand Book, 9th edition, 2000.